The current issue and full text archive of this journal is available on Emerald Insight at:
www.emeraldinsight.com/0332-1649.htm

Received 24 June 2015
Revised 24 September 2015
21 October 2015
Accepted 23 October 2015

Downloaded by Texas A&M University At 09:30 23 January 2016 (PT)

Approximation of the time-dependent induction equation with advection using Whitney elements

Application to dynamo action

Caroline Nore
LIMSI-CNRS, Paris-Sud University, Orsay, France
Houda Zaidi
CEA, Gif sur Yvette, France
Frederic Bouillault and Alain Bossavit
GeePs, Gif sur Yvette, France, and
Jean-Luc Guermond
Department of Mathematics, Texas A&M University, College Station, Texas, USA

Abstract

Purpose – The purpose of this paper is to present a new formulation for taking into account the convective term due to an imposed velocity field in the induction equation in a code based on Whitney elements called DOLMEN. Different Whitney forms are used to approximate the dependent variables. The authors study the kinematic dynamo action in a von Kármán configuration and obtain results in good agreement with those provided by another well validated code called SFEMaNS. DOLMEN is developed to investigate the dynamo action in non-axisymmetric domains like the impeller driven flow of the von Kármán Sodium (VKS) experiment. The authors show that a 3D magnetic field dominated by an axisymmetric vertical dipole can grow in a kinematic dynamo configuration using an analytical velocity field.

Design/methodology/approach – Different Whitney forms are used to approximate the dependent variables. The vector potential is discretized using first-order edge elements of the first family. The velocity is approximated by using the first-order Raviart-Thomas elements. The time stepping is done by using the Crank-Nicolson scheme.

Findings – The authors study the kinematic dynamo action in a von Kármán configuration and obtain results in good agreement with those provided by another well validated code called SFEMaNS. The authors show that a 3D magnetic field dominated by an axisymmetric vertical dipole can grow in a kinematic dynamo configuration using an analytical velocity field.

Originality/value – The findings offer a basis to a scenario for the VKS dynamo.

Keywords 3D FEM, Edge element method, Numerical simulation, Eddy current, Coupled phenomena, Maxwell's equation, Electromagnetic fields

Paper type Research paper

COMPEL: The International Journal for Computation and Mathematics in Electrical and Electronic Engineering
Vol. 35 No. 1, 2016
pp. 326-338
© Emerald Group Publishing Limited
0332-1649
DOI 10.1108/COMPEL-06-2015-0235

This work has benefited from the financial support of the LabeX LaSIPS (ANR-10-LABX-0040-LaSIPS) managed by the French National Research Agency under the Investissements d'avenir program (ANR-11-IDEX-0003-02). The HPC resources for SFEMaNS were provided by GENCI-IDRIS (grant 2014-0254) in France.

Downloaded by Texas A&M University At 09:30 23 January 2016 (PT)

1. Motivation

Still a century after Larmor suggested that dynamo action can be a source of magnetic field in planets and stars, the exact mechanism by which a fluid dynamo can be put in action in astrophysical bodies remains largely an open question. Moreover, it is only recently that fluid dynamos have been produced experimentally. For instance, in the Riga (Gailitis *et al.*, 2000) and Karlsruhe (Stieglitz and Müller, 2001) experiments, both successful in 1999, the observed magnetic field had the expected spatial distribution, namely, a non-axisymmetric equatorial dipolar structure, and the observed thresholds for dynamo action agreed with the calculations performed with simplified velocity fields and geometries. But in the successful von Kármán Sodium (VKS) dynamo experiment of September 2006 at Cadarache (see Monchaux *et al.*, 2007), the magnetic field that was observed showed a strong axisymmetric component (aligned with the symmetry axis of the set-up) that could not be predicted using simplified axisymmetric velocity fields and geometries. Moreover, dynamo action could be observed only when at least one of the rotating impellers driving the flow was made of soft iron. It is now recognized that the high magnetic permeability of the impellers plays a crucial role in the selection of the axisymmetric mode in the VKS dynamo experiment (Miralles *et al.*, 2013). The main motivation of this paper is to present a finite element technique to simulate the kinematic VKS dynamo using Whitney elements. This method is based on the software DOLMEN and uses a realistic magnetic permeability distribution and an accurate three-dimensional representation of the disk and impellers of the experiment. This new code is validated against a benchmark result and a well-documented code called SFEMaNS and therefore provides an alternative based on a different formulation. Although it is less efficient than SFEMaNS, we believe that it is more precise for modeling sharp blades fitted on a disk.

The paper is organized as follows: Section 2 presents the numerical approach used in DOLMEN and summarizes the characteristics of the SFEMaNS code that is used to validate the new algorithm; Section 3 presents a validation case of DOLMEN against a published result (Witkowski *et al.*, 2000) which can serve as a benchmark. Section 4 discusses the results obtained with two configurations of kinematic dynamo. In Section 5 we conclude by proposing a possible mechanism for the VKS dynamo action.

2. Numerical settings

The computational domain is denoted Ω and shown in Figure 3. The eddy current approximation of the Maxwell equations leads to the following set of equations:

$$\partial_t \mathbf{B} + \nabla \times \mathbf{E} = \underline{0}, \tag{1}$$

$$\nabla \times \mathbf{H} = \mathbf{J}, \tag{2}$$

$$\nabla \cdot \mathbf{B} = 0, \tag{3}$$

where ∂_t is the partial derivative with respect to time, $\mathbf{B}$ is the magnetic flux density (T), $\mathbf{E}$ is the electric field (V/m), $\mathbf{H}$ is the magnetic field (A/m) and $\mathbf{J}$ is the conduction current density (A/m). Two constitutive laws are necessary to close the system, and we use:

$$\mathbf{B} = \mu \mathbf{H}, \tag{4}$$

$$\mathbf{J} = \sigma(\mathbf{E} + \mathbf{u} \times \mathbf{B}), \tag{5}$$

Downloaded by Texas A&M University At 09:30 23 January 2016 (PT)

where $\mathbf{u}$ is the velocity field, σ is the electric conductivity (S/m) and μ is the magnetic permeability. The above system is supplemented with an initial condition $\mathbf{B}(t=0)=\mathbf{B}_0$, and the boundary conditions will be specified later.

We take as unknown the field $\mathbf{A}$ defined by $\mathbf{A}=\mathbf{A}_0-\int_0^t \mathbf{E}(\tau)\mathrm{d}\tau$ in all space (Bossavit, 1985; Ren and Razek, 2000). Thus, $\mathbf{E}=-\partial_t\mathbf{A}$ and, by definition, $\mathbf{B}=\nabla\times\mathbf{A}$ by Faraday law (1). This implyies (3). $\mathbf{A}_0$ is chosen randomly to obtain an initial magnetic field, implying $\nabla\cdot\mathbf{B}_0=0$.

After inserting the definition of $\mathbf{A}$ into (2) and using Ohm's law (5), the induction equation is reformulated as follows:

$$\nabla\times\frac{1}{\mu}\nabla\times\mathbf{A}+\sigma(\partial_t\mathbf{A}-\mathbf{u}\times\nabla\times\mathbf{A})=\underline{0}, \tag{6}$$

where $\mu=\mu_0\mu_r$ and $\sigma=\sigma_0\sigma_r$ are the magnetic permeability and electric conductivity, respectively. The quantities μ_0, μ_r, σ_0 and σ_r are the permeability of the vacuum, the relative permeability, the conductivity of the fluid and the relative conductivity, respectively. Given a characteristic length $\mathcal{L}$ and a characteristic velocity $\mathcal{U}$, the non-dimensionalized equation is obtained by multiplying (6) by $\mathcal{L}/\mathcal{U}\sigma_0$:

$$\sigma_r\partial_t\mathbf{A}+\frac{1}{R_m}\nabla\times\left(\frac{1}{\mu_r}\nabla\times\mathbf{A}\right)-\sigma_r\mathbf{u}\times\nabla\times\mathbf{A}=\underline{0} \tag{7}$$

where $R_\mathrm{m}=\sigma_0\mu_0\mathcal{L}\mathcal{U}$ is the magnetic Reynolds number measuring the ratio of inertia to magnetic diffusion. This number is the control parameter for dynamo action (i.e. generation of magnetic field by a liquid metal flow as in the Earth's outer core) and is used in the MagnetoHydroDynamics community to compare flows of various conducting fluids.

The Galerkin weighted residual formulation is obtained by multiplying the equation by test functions chosen in the appropriate functional spaces. By using the identity of the Green weak formulation of the system (7) we can write:

$$\begin{cases} \text{find } \mathbf{A}\in\mathbf{E}_1^e \text{ Such as} \\ \int_\Omega\sigma_r\partial_t\mathbf{A}\cdot\mathbf{A}'+\frac{1}{R_m}\left[\int_\Omega\frac{1}{\mu_r}\nabla\times\mathbf{A}\cdot\nabla\times\mathbf{A}'+\int_\Gamma(\mathbf{n}\times\mathbf{H})\cdot\mathbf{A}'\right] \\ -\int_\Omega\sigma_r(\mathbf{u}\times\nabla\times\mathbf{A})\cdot\mathbf{A}'=\underline{0}, \text{ in } \Omega \end{cases} \tag{8}$$

The computational domain Ω is discretized using tetrahedra and Γ is its boundary. The surface integral term depends on the problem under consideration (zero for the following dynamo computations). Whitney forms are used to approximate the dependent variables in this formulation (Bossavit, 1988a, b; Zaidi *et al.*, 2014). The vector potential $\mathbf{A}$ is discretized using first-order edge elements. The velocity is approximated by using the first-order Raviart-Thomas elements (also called face elements) for the sake of correctly modeling the velocity field for an incompressible fluid. The elementary integrals contributing to the assembly of the total matrix are then of the form $\int_V(\mathbf{W}_f\times(\nabla\times\mathbf{W}_a))\cdot\mathbf{W}_b\,\mathrm{d}v$ for each mesh cell V, where $\mathbf{W}_a$, $\mathbf{W}_b$, $\mathbf{W}_f$ designate the Whitney elements associated with the edges a and b and the face f of V, respectively. The time stepping is done by using the Crank-Nicolson scheme.

We consider an induction problem as a validation case for DOLMEN and also kinematic dynamos in this study: the velocity field is time-independent and prescribed

Downloaded by Texas A&M University At 09:30 23 January 2016 (PT)

by an analytical formula. The DOLMEN code is validated in Section 3 against a benchmark result and in Section 4 by comparing its outputs with those obtained with the code SFEMaNS (Guermond *et al.*, 2007; Guermond *et al.*, 2011). The algorithm used in SFEMaNS solves the problem using the magnetic field in the conducting region (after standard elimination of the electric field) and the scalar magnetic potential in the insulating exterior. The fields in each region are approximated by using H^1 – conforming Lagrange elements. The coupling at the interface is done by using an interior penalty method. The divergence of the magnetic induction is controlled in a negative Sobolev norm to guarantee convergence under minimal regularity (see details in Bonito and Guermond, 2011; Bonito *et al.*, 2013).

3. Validation

In this section we consider a magnetodynamic problem of induction by a solid body rotating at constant rotation embedded in an imposed magnetic field. Note that this very simple configuration may be found in many practical applications such as rotating devices or electromagnetic processing of materials. We validate DOLMEN against a published result (Witkowski *et al.*, 2000) which can serve as a benchmark. We choose identical geometrical characteristics.

We use the cylinder radius R, the solid body rotation U and the advective time R/U as scales for space, velocity and time. The unsteady problem reads (for DOLMEN):

$$\sigma_r \partial_t \mathbf{A} + \frac{1}{R_m} \nabla \times \nabla \times \mathbf{A} - \sigma_r \mathbf{u} \times \nabla \times \mathbf{A} = \underline{0}, \text{ in } \Omega \tag{9}$$

where $\mu_r = 1$ everywhere, $\sigma_r = 1$ in Ω_c (the conducting finite cylinder) and $\sigma_r = 0$ in Ω_v (the surrounding vacuum), the magnetic Reynolds number is $R_m = \mu_0 \sigma_0 RU$ and the problem is supplemented with adequate initial data. The boundary conditions are Neumann conditions at $\Gamma_v = \partial\Omega_v$.

The cylinder rotates at speed ω around the z-axis (therefore $U = R\omega$) and is submitted to a fixed horizontal magnetic field $B_0 \mathbf{e}_x$. It has radius $R = 1$ and height $L_z^c = 1.6$. The nonconducting region is a cylinder of radius $R_v = 1.6$ and height $L_z^v = 5$. In DOLMEN, the mesh size is $h = 1/50$ and the time step is $\Delta t = 510^{-2}$. The Péclet number (Hong and Ida, 1992; Allen *et al.*, 1998) is $R_m h/R$, smaller than 2 for all considered R_m.

The magnetic energy (Figure 1(a)) decreases in time with some oscillations due to reconnections happening in the conductor and then reaches an asymptotic steady value which depends on R_m. At large times, a steady electric current flows in the cylinder and creates a magnetic field which exhibits a strong extremum of the z-component on the cylinder edge ($r = 1$, $z = \pm 0.8$) as shown in Figure 1(b). This figure shows the radial profile of $B_z(r, \theta = 0, z = 0.8)$ obtained by DOLMEN, compared to that obtained in Witkowski *et al.* (2000). The agreement is satisfying, considering that the gradient of the solution is discontinuous at the edges of the cylinder.

4. Dynamo action

For the time being we consider only the kinematic situation where the velocity field is prescribed and constant. Validation of the kinematic code is a prerequisite for the full nonlinear dynamo problem where the Navier-Stokes equations including the Lorentz force are also solved. Two examples are considered in this section. We use cylindrical coordinates (r, θ, z), with the z-axis parallel to the symmetry axis of the set-up (see Figure 2), and denote the azimuthal Fourier modes by m.

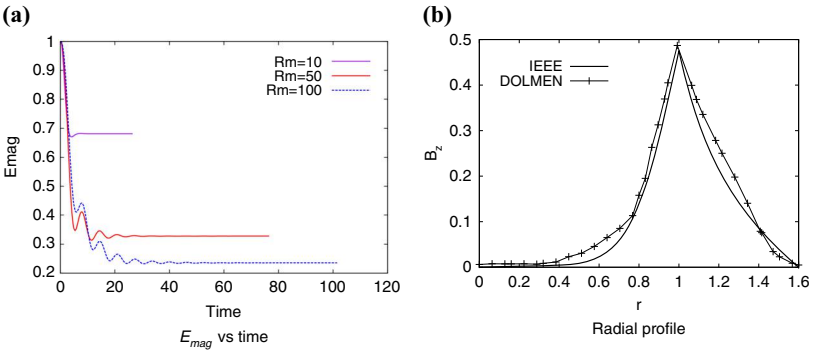

Notes: (a) Time evolution of the magnetic energy at different R_m obtained with DOLMEN; (b) radial profile of the vertical component of B_z at steady state at $z=0.8$ and $\theta=0$: "IEEE" is the result from Witkowski *et al.* (2000) (see figure 4(f) there in), and "DOLMEN" is our result with P1 Whitney finite elements ($h=1/50$ and $\Delta t=510^{-2}$, 1 point out of 2 is represented)

Figure 1.
Rotating finite cylinder

In the first configuration, both the velocity field and the heterogeneous magnetic permeability field are assumed to be axisymmetric. In this case the mode $m=0$ cannot grow due to the Cowling (1934) theorem and the mode $m=1$ is the most unstable. The results from DOLMEN are validated by comparing them with those from SFEMaNS.

In the second configuration, the velocity field is unchanged, but a realistic magnetic permeability distribution and an accurate three-dimensional representation of the disk and blades of the VKS experiment are used. The Fourier modes of the magnetic induction are coupled through the dependence of the magnetic permeability with respect to θ and disconnected families of eigenspaces can grow. Two sets of results in this configuration are presented: one corresponding to an equatorial dipole where the $m=1$ mode is dominant (the 1-family) and the other corresponding to an axial dipole

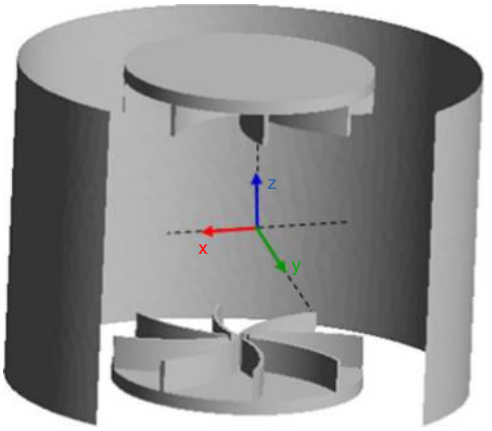

Note: The z-axis denotes the symmetry axis of the set-up

Figure 2.
Scheme of the von Kármán Sodium experiment

Downloaded by Texas A&M University At 09:30 23 January 2016 (PT)

Downloaded by Texas A&M University At 09:30 23 January 2016 (PT)

(the 0-family). Only the results from DOLMEN are presented. Those from SFEMaNS will be presented elsewhere.

4.1 Dynamo action using an axisymmetric heterogeneous magnetic permeability

We model half of the von Kármán experimental set-up (Boisson *et al.*, 2012) which is schematically represented on Figure 2.

The computational domain is a cylindrical vessel of radius $R_c = 1$ and height $h = 0.7$ ($0 \leqslant r \leqslant 1$, $-0.2 \leqslant z \leqslant 0.5$). The impeller driving the flow consists of a disk equipped with blades. The disk is a cylinder of radius $R_d = 0.54$ and height $l_d = 0.06$ ($-0.2 \leqslant z \leqslant -0.14$). The blades are modeled by a cylindrical zone of radius $R_b = 0.54$ and height $l_b = 0.14$ ($-0.14 \leqslant z \leqslant 0$). This geometry is shown in Figure 3(a).

The velocity field, $\mathbf{V}_F = (u_r, u_\theta^F, u_z)$, in the fluid ($0 \leqslant r \leqslant 1, 0 \leqslant z \leqslant 0.5$) is modeled as follows:

$$u_r = \left(\frac{\pi}{2L}\right)\cos\left(\frac{\pi z}{L}\right) r(1-r)^2(1+2r), \quad u_\theta^F = 4\varepsilon r\left(1-r^5\right)\sin\left(\frac{\pi(L-z)}{2L}\right),$$

$$u_z = -(1-r)\left(1+r-5r^2\right)\sin\left(\frac{\pi z}{L}\right), \tag{10}$$

where $L = 0.5$ denotes the distance between the top lid and the top of the blades, and ε measures the ratio between the toroidal and the poloidal components of the velocity (here, $\varepsilon = 0.7259$ as in Marié *et al.*, 2006). The velocity field in the impeller region ($0 \leqslant r \leqslant 1, -0.2 \leqslant z \leqslant 0$) is assumed to be a solid body rotation:

$$u_\theta^I = r. \tag{11}$$

The component u_θ is interpolated between the fluid region and the impeller zone using $u_\theta = u_\theta^F\left(1+\tanh(z/z_{\text{del}})\right)/(2) + u_\theta^I\left(1-\tanh(z/z_{\text{del}})\right)/(2)$, with $z_{\text{del}} = 0.05$. The flow (10) is a reasonable divergence-free approximation of the mean axisymmetric velocity field measured in water experiments using the same driving mechanisms as in the VKS experiment (Ravelet *et al.*, 2005; Marié *et al.*, 2006). The velocity field (11) assumed in the impeller region is simple: as discussed in (Ravelet *et al.*, 2008), at small kinetic Reynolds

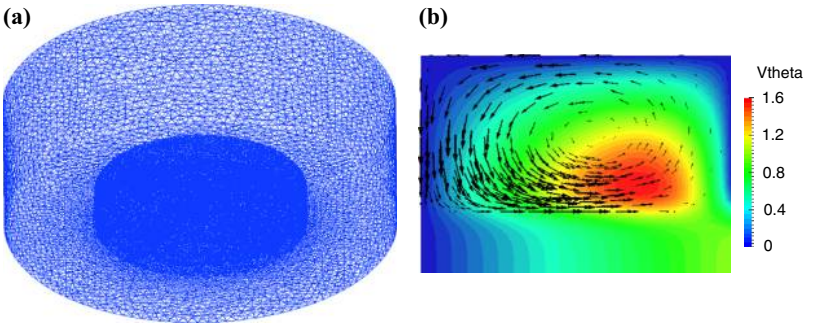

Notes: (a) Mesh used in DOLMEN computations; (b) the prescribed axisymmetric velocity field V_0 in the meridian plan $\theta = 0$. Colors represent the azimuthal velocity field component (blue/red for null/positive values) and the arrows materialize the poloidal velocity field (u_r, u_z). The left vertical edge is the symmetry axis

Figure 3.
Axisymmetric half von Kármán set-up

Downloaded by Texas A&M University At 09:30 23 January 2016 (PT)

numbers, everything goes as if the fluid was locked up between the blades leading to a solid body rotation in the impeller region.

The vector field defined above is denoted $\mathbf{V}_0$ and its maximum value is $U_{\max} = 1.66$. A meridian section of the field $\mathbf{V}_0$ is shown in Figure 3(b). All the computations presented in this paper are performed in the reference frame of the impeller, the velocity field in (7) is defined to be $\mathbf{u} := \mathbf{V}_0 - r\mathbf{e}_\theta$.

Since the vector field $\mathbf{u}$ and the geometry are axisymmetric, the terms $\mathbf{u}\times\nabla\times\mathbf{A}$ and $\nabla \times \left((1/\mu_r)\nabla \times \mathbf{A}\right)$ in Equation (7) cannot transfer energy between the Fourier modes of $\mathbf{B} = \nabla\times\mathbf{A}$, i.e., the Fourier modes are uncoupled. The boundary conditions and the initial data are chosen to enable the mode $m = 1$ to grow. The boundary conditions are defined as follows: $\mu_r^{-1}(\nabla \times \mathbf{A}) \times \mathbf{n} = 0$ (i.e. $(\mathbf{B}/\mu_r) \times \mathbf{n} = \underline{0}$, corresponding to an infinite permeability boundary) on the side of the vessel (at $r = \overline{1}$, $-0.2 \leqslant z \leqslant 0.5$) and on the bottom lid ($z = -0.2$, $0 \leqslant r \leqslant 1$), and $\mathbf{A} \times \mathbf{n} = \underline{0}$ (i.e. $\mathbf{B}.\mathbf{n} = \underline{0}$, corresponding to an infinite conductivity boundary) on the top lid (at $z = \overline{0.5}$, $0 \leqslant r \leqslant \overline{1}$). The initial condition used in this configuration is $\mathbf{B}_0 = \mathbf{e}_x$ supplemented with small amplitude noise.

The computation is carried out with the relative conductivity $\sigma_r = 1$ everywhere and with the relative permeability in the disk, $\mu_r(\text{disk}) = \mu_d$, and in the blades, $\mu_r(\text{blades}) = \mu_b$, equal to 5, both for DOLMEN and SFEMaNS. Two values of the magnetic Reynolds number are considered: $R_m = 50$ and $R_m = 70$. The time evolution of the magnetic energy $E_{\text{mag}} = (1/2)\int_\Omega \mathbf{B}\cdot\mathbf{H}dv$ is calculated with the two codes for these two values and is shown in Figure 4. The magnetic energy varies exponentially with respect to time. The slope of the logarithmic curve is calculated and subsequently a threshold R_m^c is determined at which the slope is zero. DOLMEN gives $R_m^c \approx 58.5$, whereas SFEMaNS gives $R_m^c \approx 58$; these two results are in excellent agreement.

The magnetic field near the threshold is shown on Figure 5. This mode rotates in the same direction as that of the disk and blades in the reference frame of the laboratory. It has the expected structure of a half equatorial dipole as found in Laguerre *et al.* (2006). The first bifurcation is of Hopf type: the imaginary part of the eigenvalue $2\pi/T$ is approximately 0.25, the angular velocity of the eigenmode in the reference frame of the laboratory is four times slower than that of the impeller.

4.2 Dynamo action using an analytical axisymmetric velocity field and a non-axisymmetric heterogeneous magnetic permeability

The same analytical and axisymmetric vector field $\mathbf{V}_0$ as above is used in this section, but now the real geometry of the impeller is approximated correctly, i.e., the cylinder modeling the blades in the previous section is replaced by eight curved blades. The height of the blades is $l_b = 0.14$, their thickness is $e_b = 0.02$, the angle at the rim is

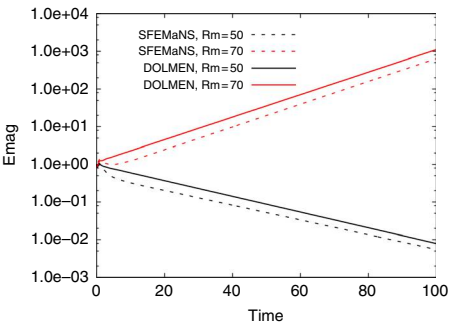

Figure 4.
Time evolution of the magnetic energy of the mode $m = 1$ in lin-log scale obtained with SFEMaNS and DOLMEN codes in the axisymmetric configuration

$\alpha = 24°$, and the generator radius is $R_g = 0.66$ (see Figure 6 (a)). The blades push the fluid with their convex side. Figure 6(b) shows the trace of the tetrahedral mesh of the impeller that is used for this case.

Due to the dependence of the magnetic permeability with respect to the azimuth angle, the eigenvalue problem associated with (7) has five disconnected families of eigenspaces. More specifically, since the magnetic permeability is supported by the Fourier modes $e^{8ik\theta}$, $k \in \mathbb{Z}$, the term $\nabla \times \left((1/\mu_r)\nabla \times \mathbf{A}\right)$ couples the modes in the following vector spaces: span$\{e^{8ik\theta}, k \in \mathbb{Z}\}$, span $\{e^{i(\pm 1 + 8k)\theta}, k \in \mathbb{Z}\}$, span $\{e^{i(\pm 2 + 8k)\theta}, k \in \mathbb{Z}\}$, span$\{e^{i(\pm 3 + 8k)\theta}, k \in \mathbb{Z}\}$ and span $\{e^{i(4 + 8k)\theta}, k \in \mathbb{Z}\}$. We henceforth refer to the above five vector spaces as the 0-family, the 1-family, etc. Given any initial data for (7) with nonzero projection on the five families, long time integration of the equation gives a magnetic field which is a superposition of the leading eigenvectors in each family. The corresponding eigenvectors are obtained by projecting the magnetic field on each of the above families.

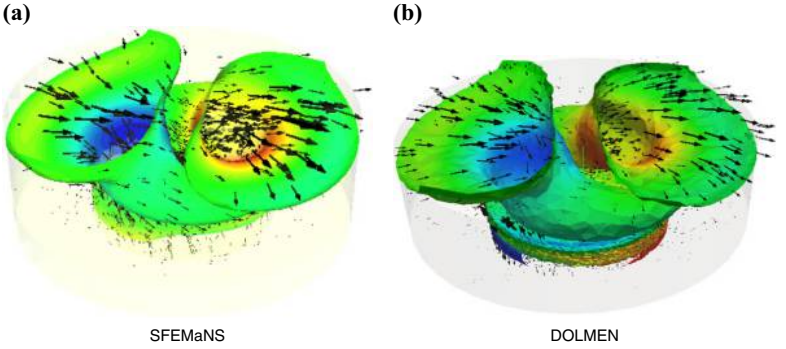

Figure 5. Rotating magnetic field obtained with an axisymmetric geometry

Notes: (Color online) Structure of the rotating magnetic field (at $R_m = 50$ with $\mu_b = \mu_d = 5$) represented by vectors and the isosurface $\|B\|^2$ (10 percent of maximum value) colored by the vertical component (minimum value in blue and maximum value in red). Notice the $m = 1$ structure

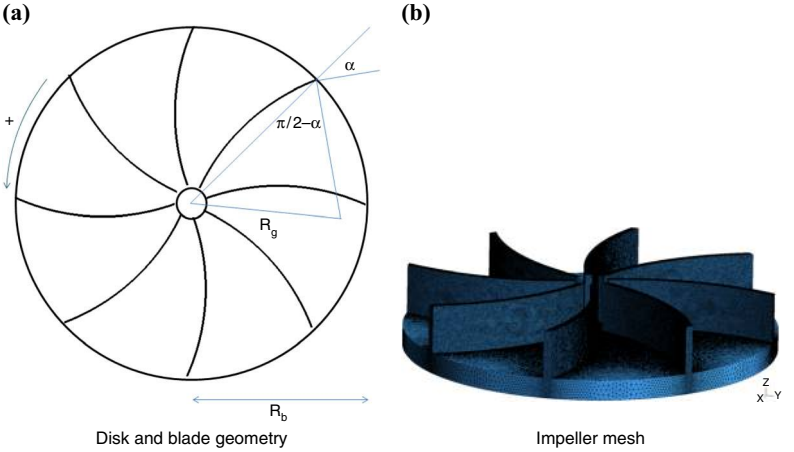

Figure 6. (a) Geometric parameters defining the blades; (b) impeller mesh used in DOLMEN for the half von Kármán set-up

Downloaded by Texas A&M University At 09:30 23 January 2016 (PT)

4.2.1 The 1-family. In this first series of computations, we use the same boundary conditions and initial data as in the previous section. With these boundary conditions, the 1-family is the leading one. The magnetic permeability in the blades and in the cylinder is $\mu_b = \mu_d = 5$. The magnetic Reynolds numbers $R_m = 50$ and $R_m = 70$ are considered and the time evolutions of the magnetic energy for these two cases are shown in Figure 7.

The measured growthrates are close to those obtained in the previous section; the threshold is only slightly increased in the bladed configuration (compare $R_m^c \approx 61$ (with blades) and $R_m^c \approx 58.5$ (no blade)). These simulations seem to show that the real geometry of the blades does not seem to have a lot of influence on the eigenmode which is localized in the bulk. This 1-family is a bulk-dynamo mode. Due to resolution restriction, we could not increase the value of μ_b and μ_d.

The structure of the magnetic field of the dominant 1-family is shown in Figure 8 (compare Figures 5 and 8(a)). The footprint on the blades is clearly visible. The rotation

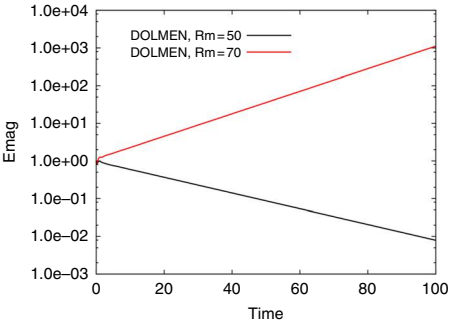

Figure 7.
Time evolution of the magnetic energy in lin-log scale obtained with DOLMEN for the non-axisymmetric configuration and the dominant 1-family

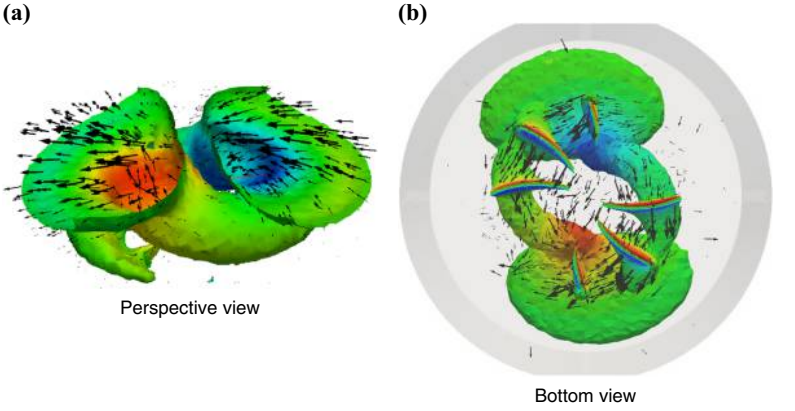

Notes: Structure of the rotating magnetic field generated in a half von Kármán set-up in the bladed configuration (at $R_m = 70$ with $\mu_b = \mu_d = 5$) represented by vectors and the isosurface $\|B\|^2$ (5 percent of maximum value) colored by the vertical component (minimum value in blue and maximum value in red) shown (a) in a perspective view and (b) from below to emphasize the blades. Notice the $m = 1$ structure of the magnetic field in the bulk and the footprint on the eight blades (DOLMEN results)

Figure 8.
Rotating magnetic field obtained with a realistic impeller

Downloaded by Texas A&M University At 09:30 23 January 2016 (PT)

of the eigenmode is retrograde in the reference frame of the impeller and its period is $2\pi/0.75$. This corresponds to a prograde rotation in the reference frame of the laboratory with a rotation period equal to $2\pi/0.25$ as in the previous section.

4.2.2 The 0-family. In this second series of computations, we change the boundary conditions: more precisely, we impose the same condition on the side and bottom lid as in the previous section, but now we impose $(\mathbf{B}/\mu_r)\times\mathbf{n}=0$ on the top lid (i.e. $\mathbf{A}\cdot\mathbf{n}=0$, corresponding to an infinite permeability boundary). The 0-family and the 2-family are the leading ones. We focus on the 0-family.

We set again $\mu_b=\mu_d=5$, and we measure the growthrate for the magnetic Reynolds numbers $R_m=\{90; 550; 750\}$ (data not shown). By extrapolation, the threshold should be $R_m^c\approx 1300$. Computations beyond the threshold have not been done due to insufficient computational ressources at the moment. The decreasing magnetic field at $R_m=90$ is shown in Figure 9 (we expect the growing magnetic field to have the same structure). It is steady. Note that the magnetic field is mainly azimuthal and axisymmetric in the disk (which can be considered as a reservoir of toroidal field), it is concentrated in the blades (where it is poloidal and non-axisymmetric), and it is mainly axial and axisymmetric in the bulk. This structure is very similar to the measured growing magnetic field reported in Boisson *et al.* (2012).

Based on the structure of this 0-family magnetic field, we propose a mechanism for the dynamo action based on four steps: first, the ω-effect generates a toroidal magnetic

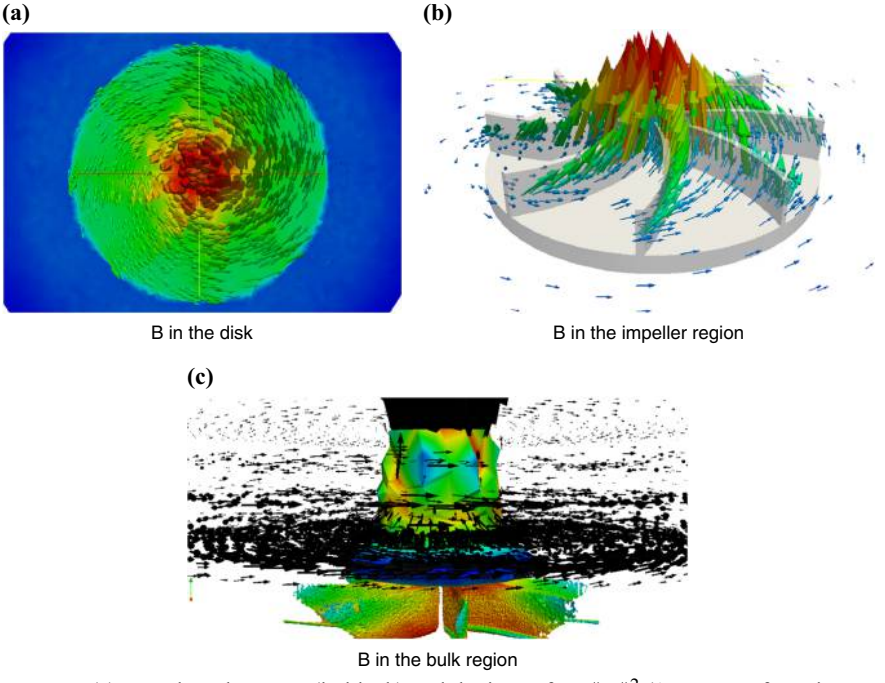

Note: In (c), are plotted vectors (in black) and the isosurface $\|B\|^2$ (1 percent of maximum value – colored by the vertical component with minimum value in blue and maximum value in red)

Figure 9.
Structure of the 0-family magnetic field generated in a half von Kármán set-up with the velocity field $\mathbf{V}_0$ (at $R_m=90$ with $\mu_b=\mu_d=5$) represented by vectors (colored by the vertical component) shown (a) in the disk, (b) in the impeller region and (c) in the bulk region

Downloaded by Texas A&M University At 09:30 23 January 2016 (PT)

field from poloidal magnetic field seeds; second, this azimuthal magnetic field is stored in the high permeability disk (cf. Giesecke *et al.*, 2012) as in Figure 9(a); third, this azimuthal field is collected in the blades and transformed into a poloidal field as in Figure 9(b) and; fourth, focussing of the poloidal components gives rise to the vertical component on the axis as in Figure 9(c).

5. Conclusions

A new formulation taking into account the convective term of the induction equation has been validated in the code DOLMEN. We have been able to model the azimuthal variation of the magnetic permeability of a real impeller (disk and curved blades) and we have shown that a mainly axisymmetric eigenmode might grow in a kinematic dynamo configuration using an analytical velocity field.

Downloaded by Texas A&M University At 09:30 23 January 2016 (PT)

References

Allen, N., Lai, H., Rodger, D. and Leonard, P. (1998), "On the validity of two A-Psi finite element formulations for modelling eddy current problems with velocity", *IEEE Transactions on Magnetics*, Vol. 34 No. 5, pp. 2535-2538.

Boisson, J., Aumaitre, S., Bonnefoy, N., Bourgoin, M., Daviaud, F., Dubrulle, B., Odier, P., Pinton, J.-F., Plihon, N. and Verhille, G. (2012), "Symmetry and couplings in stationary von Kármán sodium dynamos", *New Journal of Physics*, Vol. 14 No. 1, pp. 1-18.

Bonito, A. and Guermond, J.-L. (2011), "Approximation of the eigenvalue problem for the time harmonic Maxwell system by continuous Lagrange finite elements", *Mathematics of Computation*, Vol. 80 No. 276, pp. 1887-1910.

Bonito, A., Guermond, J.-L. and Luddens, F. (2013), "Regularity of the Maxwell equations in heterogeneous media and Lipschitz domains", *Journal of Mathematical Analysis and Applications*, Vol. 408 No. 2, pp. 498-512.

Bossavit, A. (1985), "Two dual formulations of the 3D eddy-currents problem", *COMPEL – The International Journal for Computation and Mathematics in Electrical and Electronic Engineering*, Vol. 4 No. 2, pp. 103-116.

Bossavit, A. (1988a), "A rationale for 'edge-elements' in 3-D fields computations", *IEEE Transactions, MAG-24*, Vol. 24 No. 1, pp. 74-79.

Bossavit, A. (1988b), "Whitney forms: a class of finite elements for three-dimensional computations in electromagnetism", *Physical Science, Measurement and Instrumentation, Management and Education – Reviews, IEE Proceedings A*, Vol. 135 No. 8, pp. 493-500.

Cowling, T. (1934), "The magnetic field of sunspots", *Monthly Notices of the Royal Astronomical Society*, Vol. 94 No. 1, pp. 39-48.

Gailitis, A., Lielausis, O., Dement'ev, S., Platacis, E. and Cifersons, A. (2000), "Detection of a flow induced magnetic field eigenmode in the Riga dynamo facility", *Physical Review Letters*, Vol. 84 No. 19, pp. 4365-4368.

Giesecke, A., Nore, C., Stefani, F., Gerbeth, G., Léorat, J., Herreman, W., Luddens, F. and Guermond, J.-L. (2012), "Influence of high-permeability discs in an axisymmetric model of the Cadarache dynamo experiment", *New Journal of Physics*, Vol. 14 No. 5, pp. 1-16.

Guermond, J.-L., Laguerre, R., Léorat, J. and Nore, C. (2007), "An interior penalty Galerkin method for the MHD equations in heterogeneous domains", *Journal of Computational Physics*, Vol. 221 No. 1, pp. 349-369.

Guermond, J.-L., Léorat, J., Luddens, F., Nore, C. and Ribeiro, A. (2011), "Effects of discontinuous magnetic permeability on magnetodynamic problems", *Journal of Computational Physics*, Vol. 230 No. 16, pp. 6299-6319.

Hong, S. and Ida, N. (1992), "Modeling of velocity terms in 3D eddy current problems", *IEEE Transactions on Magnetics*, Vol. 28 No. 2, pp. 1178-1181.

Laguerre, R., Nore, C., Léorat, J. and Guermond, J.-L. (2006), "Effects of conductivity jumps in the envelope of a kinematic dynamo flow", *CR Mécanique*, Vol. 334 No. 10, pp. 593-598.

Marié, L., Normand, C. and Daviaud, F. (2006), "Galerkin analysis of kinematic dynamos in the von Kármán geometry", *Physics of Fluids*, Vol. 18 No. 1, pp. 1-18.

Miralles, S., Bonnefoy, N., Bourgoin, M., Odier, P., Pinton, J.-F., Plihon, N., Verhille, G., Boisson, J., Daviaud, F. and Dubrulle, B. (2013), "Dynamo threshold detection in the von Kármán sodium experiment", *Physical Review E*, Vol. 88 No. 1, pp. 1-12.

Monchaux, R., Berhanu, M., Bourgoin, M., Odier, P., Moulin, M., Pinton, J.-F., Volk, R., Fauve, S., Mordant, N., Pétrélis, F., Chiffaudel, A., Daviaud, F., Dubrulle, B., Gasquet, C., Marié, L. and Ravelet, F. (2007), "Generation of magnetic field by a turbulent flow of liquid sodium", *Physical Review Letters*, Vol. 98 No. 4, pp. 1-4.

Ravelet, F., Chiffaudel, A. and Daviaud, F. (2008), "Supercritical transition to turbulence in an inertially driven von Kármán closed flow", *Journal of Fluid Mechanics*, Vol. 601, pp. 339-364.

Ravelet, F., Chiffaudel, A., Daviaud, F. and Léorat, J. (2005), "Towards an experimental von Kármán dynamo: numerical studies for an optimized design", *Physics of Fluids*, Vol. 17, pp. 1-17.

Ren, Z. and Razek, A. (2000), "Comparison of some 3D eddy current formulations in dual systems", *IEEE Transactions on Magnetics*, Vol. 36 No. 4, p. 751-755.

Stieglitz, R. and Müller, U. (2001), "Experimental demonstration of a homogeneous two-scale dynamo", *Physics of Fluids*, Vol. 13 No. 3, pp. 561-564.

Witkowski, L.M., Marty, P. and Walker, J. (2000), "Multidomain analytical-numerical solution for a rotating magnetic field with finite-length conducting cylinder", *IEEE Transactions on Magnetics*, Vol. 36 No. 2, pp. 452-460.

Zaidi, H., Nore, C., Bossavit, A., Bouillault, F. and Guermond, J.-L. (2014), "Whitney element approach for dynamo action modeling with a von Kármán type velocity", *Sixth biennal IEEE Conference on Electromagnetic Field Computation, May, Annecy*, Poster PA3:9.

About the authors

Caroline Nore graduated from the Ecole Normale Supérieure de Lyon in 1992 and received a PhD Degree from the Paris Descartes University in 1995. She joined the Laboratoire d'Informatique pour la Mécanique et les Sciences de l'Ingénieur in 1996. She obtained the habilitation dissertation in 2003 from the University Paris-Sud. She is a Professor in the physics department at the University Paris-Sud since 2007. Her research interests concern Fluid mechanics, MagnetoHydrodynamics, bifurcation and numerical modeling.

Houda Zaidi obtained in 2008 her Master's Degree 1 in Mathematics and Applications at the University of Monastir (ISIMM), Tunisia. In 2009, she obtained the Master's Degree 2 in numerical analysis and modeling from the University of Picardie Jules Verne. In December 2012, she had her PhD Degree from the University of Paris-Sud. During her thesis she worked on the modeling of electromagnetic non-destructive testing by the finite element method. Currently she has a Postdoctoral position at the CEA.

Professor Frederic Bouillault graduated from the Ecole Normale Supérieure de Cachan and received a PhD Degree from the University of Paris-Sud in 1984. Since 1980 he works at electrical laboratory in Paris, which became GeePs in 2015, associated with the CNRS, Supélec and the Universities of Paris. From 2006 to 2015, he managed the laboratory. He is currently a Professor. His research interests are numerical modeling of electromagnetic phenomena. Professor Frederic Bouillault is the corresponding author and can be contacted at: bouillault@lgep.supelec.fr

Downloaded by Texas A&M University At 09:30 23 January 2016 (PT)

Dr Alain Bossavit earned a PhD in Numerical Analysis in 1970 and worked at the Research Division of Electricité de France till 2002, when he retired from his last position as a Scientific Adviser. He is now with the GeePs laboratory (Electrical Engineering Group) of the Paris-Saclay University. His main current interests are metamaterials and electromagnetic forces.

Jean-Luc Guermond graduated from the ENSTA in 1983 and received a PhD Degree from the UPMC in 1985. He was a Research Associate at the Bassin d'Essais des Carènes, Paris, France, in 1984, CNRS Research Scientist at the Laboratoire d'Informatique pour la Mécanique et les Sciences de l'Ingénieur in 1990 and CNRS Directeur de Recherches in 2001. He obtained the habilitation dissertation in 1995 from the UPMC. He is a Professor at the Department of Mathematics, Texas A&M, College Station, USA. His research interests concern fluid flows, turbulence, Navier-Stokes equations, magneto hydrodynamics, Maxwell equations, numerical analysis.

Downloaded by Texas A&M University At 09:30 23 January 2016 (PT)

For instructions on how to order reprints of this article, please visit our website:
www.emeraldgrouppublishing.com/licensing/reprints.htm
Or contact us for further details: **permissions@emeraldinsight.com**